Materials Research. 2023; 26:e20230187
DOI: https://doi.org/10.1590/1980-5373-MR-2023-0187

Study of the Optoelectronic Properties of Titanium Nitride Thin Films Deposited on Glass by Reactive Sputtering in the Cathodic Cage

Hunos Paixão Madureira[a], Renan Matos Monção[a], Adriano Almeida Silva[b], Angel Alberto Hidalgo[c], Maria Letícia Vega[b], Michelle Cequeira Feitor[d], Francisco Eroni Paz Santos[a,b], Thércio Henrique de Carvalho Costa[d]*, Rômulo Ribeiro Magalhães de Sousa[a]

[a]Universidade Federal do Piauí (UFPI), Programa de Pós-Graduação em Ciência e Engenharia dos Materiais, Teresina, PI, Brasil.
[b]Universidade Federal do Piauí (UFPI), Programa de Pós-Graduação em Física,Teresina, PI, Brasil.
[c]Universidade Federal do Piauí (UFPI), Departamento de Física, Teresina, PI, Brasil.
[d]Universidade Federal do Rio Grande do Norte (UFRN), Programa de Pós-Graduação em Engenharia Mecânica, Natal, RN, Brasil.

Received: March 28, 2023; Revised: July 24, 2023; Accepted: September 14, 2023

We investigate the structural, optical, thermal-optical, and electronic properties of TiN_x thin films utilizing a variety of experimental techniques, including spectroscopic ellipsometry, Raman spectroscopy, scanning electron microscopy, atomic force microscopy, thermal lens spectroscopy, and UV-VIS spectroscopy. Our experimental results indicate a remarkable metallic character in the TiN_x thin films deposited under lower N_2 flow during treatment, as well as an increase in reflectance in the infrared region and thermal diffusivity as the partial N_2 flow is reduced, which is consistent with previous experimental studies. The microscopic origin of these trends is explained in terms of the atomic structure of the system, where Ti atoms contribute free carriers that interact with IR radiation and N atoms create imperfections in the lattice, causing greater scattering of phonons, respectively. The experimental results also indicate that the roughness of the films produced with a lower N_2 partial flow was lower than that of the films with a higher N_2 partial flow. To explain the deviation of optical properties from the ideal case, surface oxidation is also investigated. This facilitates the coating of smarting windows with TiNx thin films.

Keywords: *Plasma Deposition, Cathode Cage, Titanium Nitride, Thin Films.*

1. Introduction

The continuous use of fossil fuels is one of the main factors that intensify global warming and environmental pollution. In addition, the depletion of non-renewable resources essential for the continuous development and production of technologies that help solve problems and improve humanity's living conditions stimulate the search and development of new materials and alternative technologies that effectively replace their precedents[1-5]. Innovating to minimize energy use while achieving the same or better results is significant to tackle the core of the problem: the massive use of fossil fuels and the growing need for electricity. To slow the destructive effects of global warming, energy-efficient buildings, vehicles, and windows are gaining increasing attention, as an indoor environment kept warm or cold with little or no electricity affects energy consumption[1-6].

Used as a coating for windows in homes, buildings, and vehicles with materials in the visible spectrum and with reflectance in the infrared range, the thermoregulatory material is a viable strategy as a starting point to reduce the consumption of electricity spent on heating and heating lighting[1-7]. Titanium nitride (TiN) is included in the transition metal nitride set that presents remarkable resistance to several factors, such as extreme temperature and pressure conditions, and durability capable of being used in multiple technological areas, from cutting tools to rocket parts[8,9]. TiN thin films have been widely studied in recent decades, given their importance and applicability in several commercial areas due to the combination of their mechanical properties - high melting point, hardness, corrosion resistance - and optoelectronic properties, which derive from the metallic behavior of free electrons existing in the d-band of Ti. TiN can also be applied as a heat mirror, as it is very stable when subjected to high temperatures and highly reflective in the near-infrared region[7,10-12].

The production of thin films by sputtering is a recent technique derived from the sputtering deposition method. A cylindrical cage, composed of the material to be deposited, houses the substrate inside, and both are positioned in the cathode reactor. The new technique, developed and patented by the Plasma Materials Processing Laboratory of the Federal University of Rio Grande do Norte (UFRN) (PI0603213-3) in 2007, has advantages that make it viable and effective, including the elimination of the edge effect and overheating that commonly occur in plasma nitriding processes, use in some of the existing deposition equipment, high film deposition rate, etc.

*e-mail: thercioc@hotmail.com

Bilokur et al.[13] investigated the optical properties of TiN, AlON, and TiAlN thin films deposited on glass and Si. The authors report that stoichiometric TiN has high reflectance in the infrared and low in the visible light spectrum. However, the best results for the spectral selectivity property occurred in films where the combination of dielectric, semiconductor, and conductor materials in multiple layers was performed.

In this work, cathodic cage plasma deposition (CCPD) will be performed varying nitrogen flow to produce thin TiN films on glass substrates. The results should contribute to discussing the relevance and applicability of TiN as a functional solar selective coating for energy-saving technology applications.

2. Materials and Methods

In this study, we used as substrate microscopic glass plates cut in the dimensions of 25.4 x 12.3 mm and 1 mm thick, where we deposited TiN_x thin films through the method of plasma deposition in a cathodic cage. Table 1[14] and Table 2 show the chemical composition of the substrates and the cathode cage, respectively.

The cathode cage was milled from a titanium sheet, and its dimensions are 80 mm (height) × 100 mm (Ø), with evenly spaced holes of 10 mm (Ø) and center-to-center spacing of 20 mm, and sanded with 600 mesh sandpaper. The cathodic cage and the samples were cleaned by immersion in nitric acid, washed in running water, and immersed in acetone under ultrasonic agitation, followed by a conventional dryer. After this process, the substrates and the cage were placed in the treatment chamber.

The equipment used for plasma thin film deposition consists of a direct voltage source with maximum voltage and current of 1200 V and 2 A, respectively, and a stainless steel chamber 30 cm in diameter and 40 cm in height. Plasma is formed in the cathode cage, which acts as the cathode (the chamber lid is the anode). The samples remained at floating potential because they were positioned on an insulating surface, alumina.

The samples underwent a pre-sputtering phase for 1 hour at 350 °C in a gaseous mixture of Ar/H_2 in the ratio of 2:1 (Ar: 20 sccm; H_2: 10 sccm) to remove oxides and impurities from the surface of the cage. The sputtering phase lasted for 4 hours. The samples were subjected to treatment temperatures of 400 °C, where the proportion of the gas mixture was varied according to Tables 3 and 4 to observe how the characteristics of the films would change according to the different treatment parameters.

Raman spectra were obtained with a Bruker Senterra mono-array spectrometer equipped with a charge-coupled device (CCD) as a detection system, and the samples were excited using a solid-state laser (785 nm) with a power of 50 mW. The scanning electron microscope (SEM) from EMPRESA FEI, model QUANTA FEG 250, was used to evaluate the thickness and morphology of the deposited layers. Ten thickness measurements were taken along the length of the layers to obtain mean values and their standard deviations.

Table 1. Chemical composition of substrates.

Substance	SiO_2	Na_2O	CaO	MgO	Al_2O_3	K_2O	SO_3	F_2O_3	TiO
(%)	72.15	14.25	6.25	4.1	1.12	1.15	0.3	0.3	0.05

Source: Ye et al.[14].

Table 2. Chemical composition of the cathodic cage (Ti level 2).

Substance		Ti	C	Fe	O	H	N
Quantity (%)	**Min.**	99.055	0	0	0	0	0
	Max.	-	0.08	0.3	0.25	0.015	0.03

Source: REALUM[15].

Table 3. Sample pre-treatment conditions.

Samples	Presputtering							
	Ar (sccm)	H_2 (sccm)	Time (h)	Temperature (ºC)	Pressure (Pa)	DDP (V)	i (A)	Power (W)
A4	20	10	1	350	1400	760	37	295
A5								
A8								

Table 4. Sample treatment conditions.

Samples	Sputtering									
	Ar (sccm)	N_2 (sccm)	H_2 (sccm)	% N_2	Time (h)	Temperature (ºC)	Pressure (Pa)	DDP (V)	i (A)	Power (W)
A4	135	15	0	10	4	400	1000	544	0.58	316
A5	127	33	0	22			1000	530	0.53	282
A8	75	75	0	50			1300	551	0.53	290

The roughness and morphology of the deposited films were evaluated by measurements performed in atomic force microscopy (AFM) NTEGRA Spectra in semi-contact mode. In each sample, five measurements were performed in different regions. The area was 100, 25, and 9 μm^2 digitized with a sweep frequency of 0.78 Hz. Each image was acquired with 512x512 pixels.

A Shimadzu UV 3600 spectrophotometer with a deuterium-tungsten excitation source together with the UV-Probe-233 software was used to measure the reflectance (R) and transmittance (T) of samples prepared in glass in the spectral range of 200 to 1600 nm. The optoelectronic properties of TiN_x thin films were verified through spectroscopic ellipsometry in a Semilab GES-5E ellipsometer. A polarizer was used before the light source to generate a spectrum of polarized white light. A Drude Lorentz Tauc-Lorentz dielectric analysis based on the free electron and oscillator model was performed to investigate the relationship between nitrogen flux during thin film deposition and the behavior of its optoelectronic properties.

TLS measurements were performed using a dual beam mismatched beam setup, as detailed by Shen et al.[16]. The excitation laser employed a diode laser operating at 532 nm, while the probe beam utilized a He-Ne laser at 633 nm. TLS measurements were recorded in the transient regime, where the θ (phase difference) and tc (characteristic time) parameters were obtained from transient curves using a theoretical fit based on the TL equation (Equation 1), where m = 15.089 and V = 2.092 were used as fixed parameters, obtained from the calibration sample. Thermal diffusivity was calculated using Equation 2, using the fitted values of the curves from Equation 1, which are (t_c) and ω_e = 3.72 × 10^{-3} cm. All TLS ratios were performed at the same power, and the probe beam power was to adjust effects and not induce thermal effects.

Intensity equation.

$$I(t) = I(0)\left\{1 - \frac{\theta}{2}\tan^{-1}\left[\frac{2mV}{\left((1+2m)^2+V^2\right)\left(\frac{t_c}{2t}\right)+1+2m+V^2}\right]\right\}^2 \quad (1)$$

Thermal diffusivity equation.

$$D = \left(\frac{\omega_e^2}{4t_c}\right) \quad (2)$$

3. Results and Discussion

The Raman pattern shown in Figure 1 indicates typical titanium nitride films deposited on glass samples under all treatment conditions. The Raman peaks found in the regions between 150 and 350 cm^{-1} and between 450 and 700 cm^{-1} confirm the presence of TiN. These regions are related to vibrations of heavy Ti and light N ions, respectively, due to Ti and N vacancies in the crystal lattice. The peaks of 163, 360, 486, and 615 cm^{-1} observed in the spectra refer to transverse acoustic (TA), longitudinal acoustic (LA), transverse optical (TO), and longitudinal optical (LO) modes, respectively, and refer to first-order Raman vibration[17-19].

In order to quantify and understand the observed changes in the Raman spectrum, these were adjusted through the Lorentzian model, as shown in Figure 1. The adjustment of the Raman spectrum was used to obtain the N/Ti ratio present in the films through the peak areas, calculation of the ratio (TO+LO) / (TA+LA)[18,19]. The influence of partial N_2 flow on the N/Ti ratio is shown in Figure 2. It is observed that the addition of N_2 during film deposition follows a decrease in its N/Ti ratio, which is the opposite of what is reported in the literature[20-22].

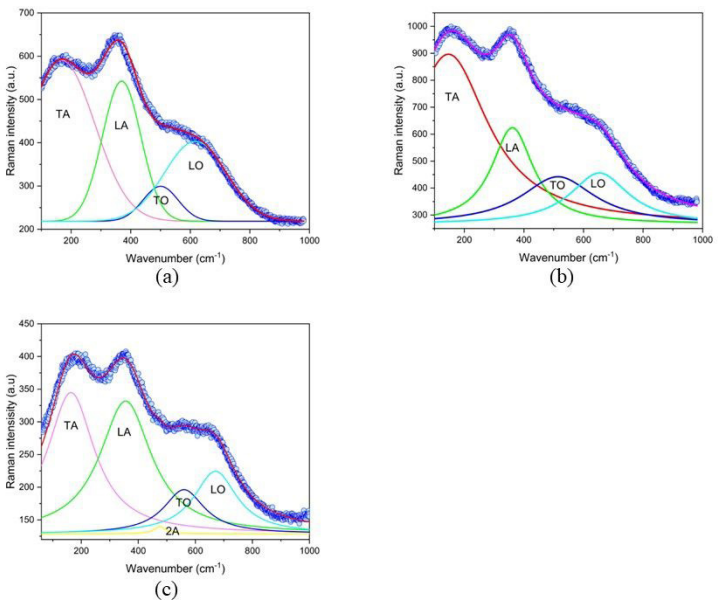

Figure 1. Raman spectrum of TiNx thin films deposited under partial N_2 flow variation and the adjustment performed on these: A4 (a), A5 (b), and A8 (c).

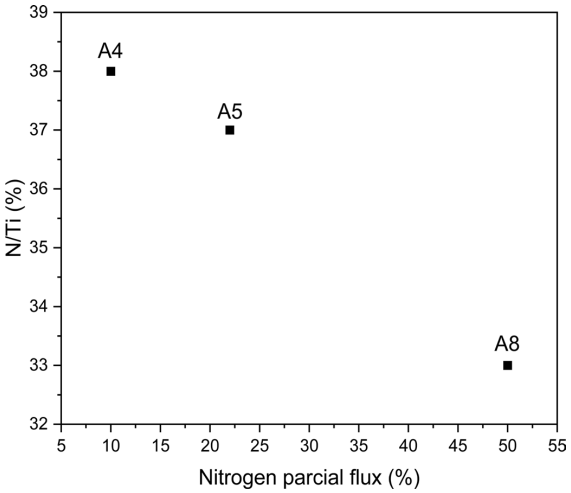

Figure 2. Relationship of dependence between the N/Ti ratio of the deposited TiN_x films and the partial flow of N_2 during deposition: A4 (a), A5 (b), and A8 (a).

Figure 3 shows cross-sectional SEM micrographs of samples treated with different proportions of Ar and N_2, indicating that all treatments resulted in the formation of a surface layer. The average film thicknesses are listed in Table 5. They show that the layer thickness increases with increasing N2/Air ratio during Cathodic Cage Plasma Deposition (CCPD). Thus, the A4 sample had the most negligible thickness, while the A8 was the largest. The increase in the mean thickness that accompanies the growth of the N_2 flow is contrary to that found in studies that do not use a cathodic cage as a target, and this shows that the proportional increase in the N_2 flow decreases the deposition rate because, due to the "poisoning" of the target resulting from the formation of TiN on its surface, the performance of the reactive spraying decreases[23-27].

The uniformity of the deposited layer, indicated by the standard deviation of the average thickness of the films, also grew along with the N/Ti ratio, showing medium to high values. This indicates that nitrogen in the films contributes to forming more uniform films, which is corroborated by the literature[28-30].

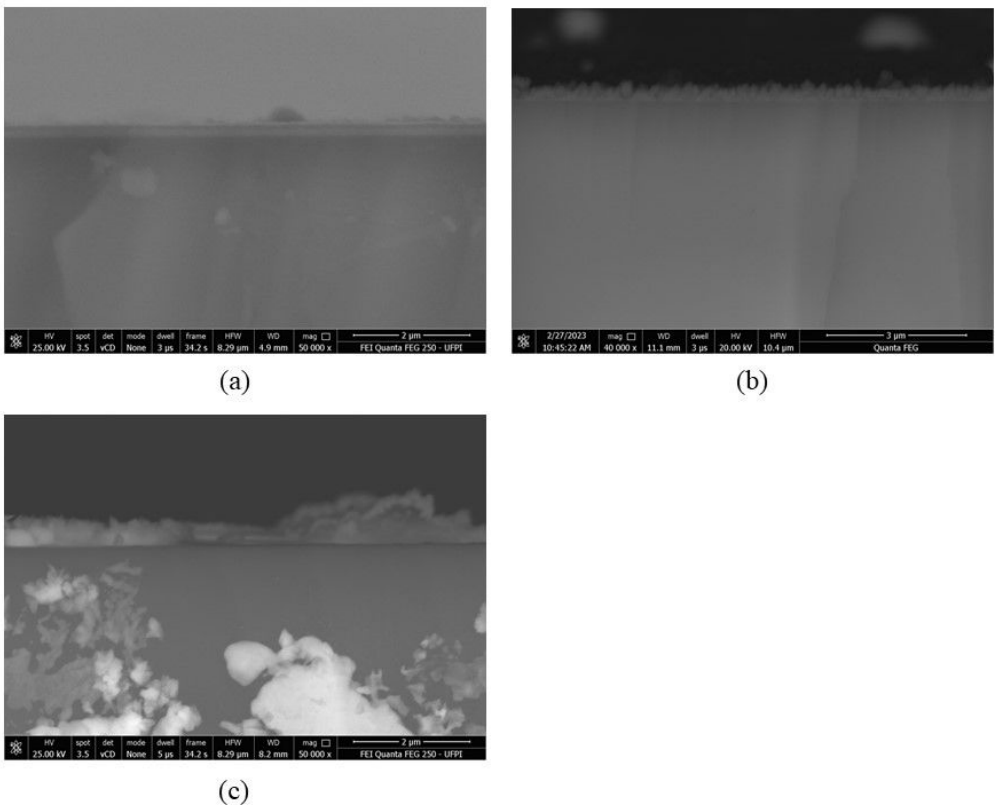

Figure 3. Electron micrographs of the cross-section and the top of the samples A4 (a), A5 (b), and A8 (c).

Table 5. N/Ti ratio was found through Raman spectroscopy, average thickness and estimate of uniformity (S) obtained through SEM measurements, and roughness (σ_{RMS}) obtained through AFM measurements of the deposited films.

Samples	N/Ti (%)	Medium thickness (nm)	Standard Deviation (SD)	σ_{RMS} (nm)
A4	38	233.1	20.29	26±12
A5	37	269.3	54.23	-
A8	33	480.7	92.37	45±7

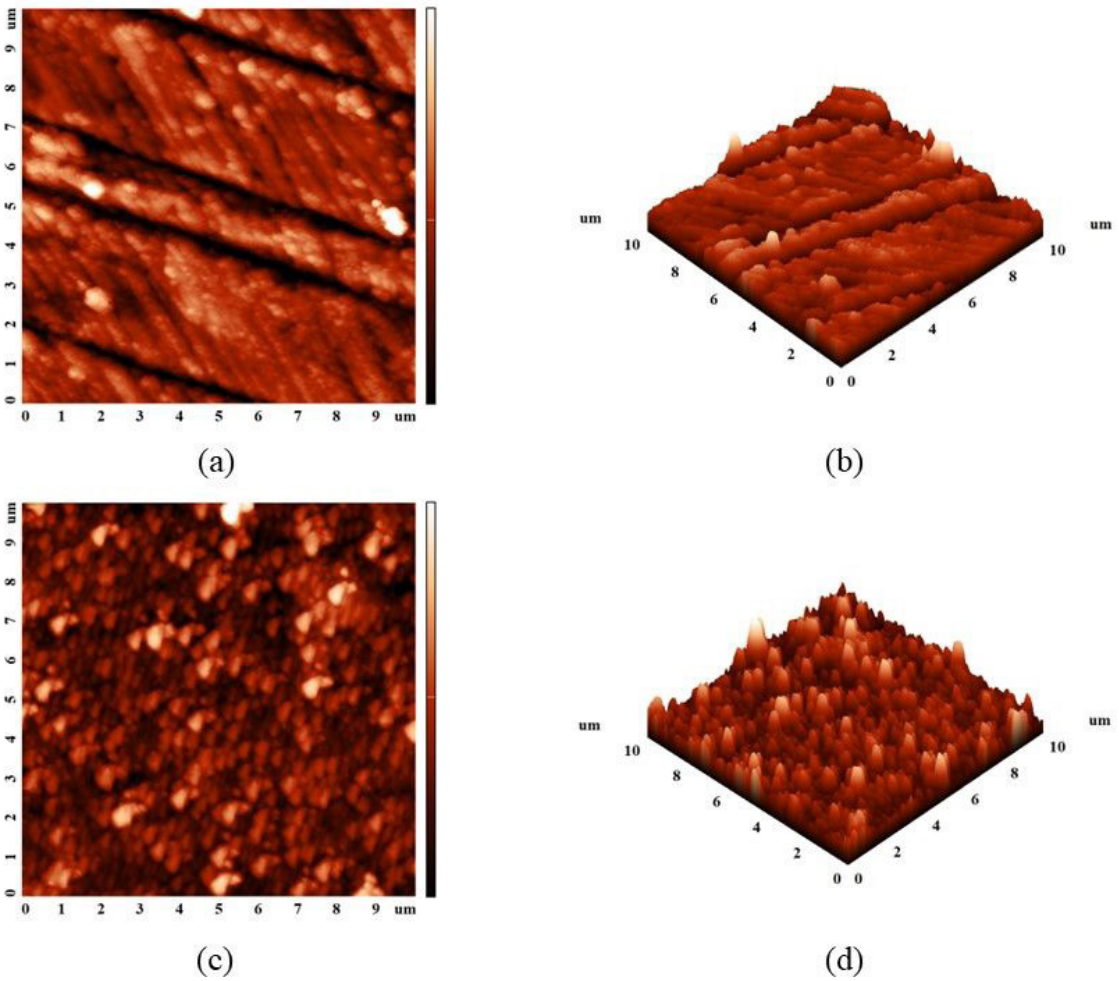

Figure 4. Images of A4 (2D (a) and 3D (b)) and A8 (2D (c) and 3D (d)) samples.

However, the increase in the flow of N_2 during deposition contributes to the non-uniformity of the films[31].

From the observation of 2D and 3D AFM images with a scan size of 9 × 9 μm² of samples A4 and A8 in Figure 4, it is evident that the films grew on the surface of the substrate by nucleation and that the roughness increased considerably as the stoichiometry decreased. Samples A4 and A8 showed roughness values of 26 nm and 45 nm, respectively. It is observed that the increase in roughness is accompanied by a decrease in the N/Ti ratio, thus being a result compatible with the literature and with previous results obtained from SEM micrographs. Surface energy, deposition time, and relative gas concentration influence grain size[25,32,33].

The data obtained through UV-VIS-NIR spectroscopy measurements show that the film that came closest to stoichiometry (sample A4 – deposited with the lowest N_2/Ar flow) was the one that exhibited the highest reflectance, mainly in the near-infrared region with a value of 30% at 1600 nm. Stoichiometric TiN reflectance is reported in a range of 70-95% depending on the deposition method and parameters and the substrate[34,35]. The reflectance results are illustrated and represented in Figure 5.

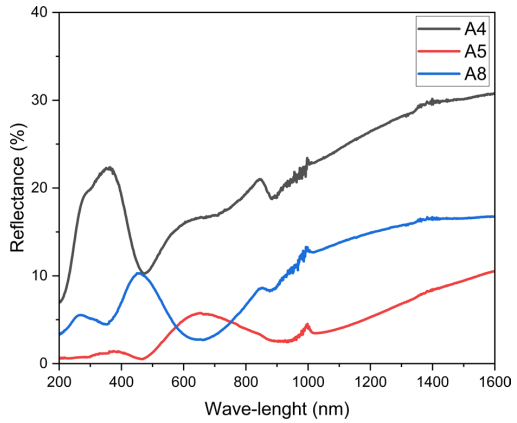

Figure 5. Specular reflectance spectra of TiN_x thin films deposited on glass substrates: A4, A5, and A8 samples.

The literature shows that a high N/Ti ratio in TiN films is accompanied by low reflectance. This is due to nitrogen capturing free electrons from titanium resulting in a decrease in light reflected by the film as the N/Ti ratio increases[34,36-38].

It has also been reported that the reflectance of stoichiometric TiN films is much higher than that of sub-stoichiometric films[39]. We believe this phenomenon occurs from the point at which the films migrate from stoichiometric to super stoichiometric. In contrast, in sub-stoichiometric films, such as those presented in this work, the reflectance increases as they approach stoichiometry since the literature also reports that stoichiometric TiN films present much higher reflectance than non-stoichiometric ones[39]. Because the thickness of the films also influences this property, where it is lower in thicker films (sample A8) and higher in thinner ones (sample A4)[39].

UV-VIS-NIR spectroscopy also provided Figure 6, from which it can be concluded that the transmittance decreases as the N_2 flow decreases, which leads us to believe that the increase in N_2 during deposition, or the decrease in the N/Ti ratio, contributed to the increase in transmittance, mainly in the visible and near-infrared spectral region. The flow of N_2 during deposition leads to a departure from the stoichiometry of the films, given the direct relationship and marked difference between the high infrared transmittance and the non-stoichiometric growth of the TiN_x films. At the same time, the UV and IR region is wholly blocked in stoichiometric films[36,40].

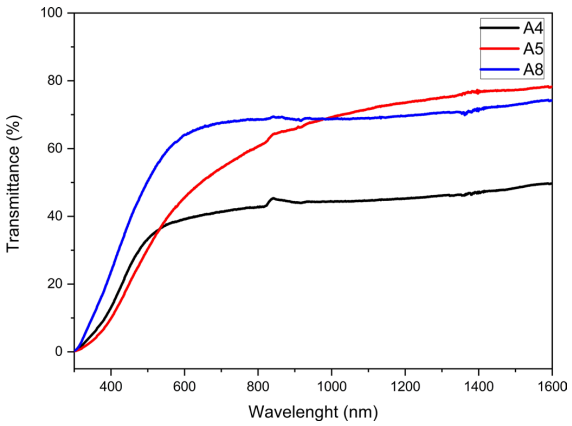

Figure 6. Spectral transmittance spectra of TiN_x thin films deposited on glass substrates: A4, A5, and A8 samples.

However, it is known that the thickness and roughness of the films also influence the reflectance and transmittance properties in such a way that the increase in thickness (sample A8 has greater thickness and roughness) results in a decrease in reflectance and transmittance (sample A8 has lower reflectance)[39,41,42].

The optoelectronic parameters TiON and TiO_2 were used to guide the phase 2 adjustment of the A4 and A8 samples, thus improving the consistency of the models applied to these films[43,44]. The average thickness and roughness of the deposited films, obtained by SEM and AFM, respectively, were used as a fixed parameter during the adjustments of the ellipsometric measurements to build a more consistent model. The quality of the fits can be seen in Figures 7 and 8 as well as in Tables 6, 7, and 8. Optically, the films are divided into layers and substrate, as shown in Figure 7. Each layer was assigned two or more dispersion laws (Drude, Lorentz, and Tauc-Lorentz models).

The ellipsometric measurements showed Lorentz bands in the ultraviolet and visible spectral regions. These bands explain that we do not see significant reflectance or transmittance in this spectral region. Thus, these bands show absorption in this region, specifically the Lorentz bands at 2.14 eV (phase 1 - Lorentz 1), 2.6 eV (phase 2), and 5.64 eV (phase 1 - Lorentz 2) eV for sample A4, 2.07 eV (phase 1 - Lorentz 2), 4.08 eV (phase 1 - Lorentz 1) and 4.2 eV(phase 2) for sample A8, being related to the absorption of light in this range, as shown in Tables 6, 7 and 8. Through the Drude model, the plasma energy of the samples was verified. The value of this parameter for sample A4 was 4.43 eV, followed by sample A8, which presented a value of 3.53 eV, as shown in Table 6. These values are within the range reported in the literature ranging from 2.6 eV for stoichiometric TiN - and above 2.6 eV for super stoichiometric TiN_x ($x > 1$)[45,46] - and 5.45 eV[47,48]. Table 9 shows the parameters derived from the ellipsometric adjustments made where sample A4 presented higher electrical conductivity and electrical resistivity lower than sample A8. Therefore, it was verified that films closer to stoichiometry are better electrical conductors when compared to those more distant from stoichiometry.

Figure 9 illustrates the thermal lens signal observed for films A4, A5, and A8 which were deposited onto glass substrates in atmospheres with different percentages of nitrogen.

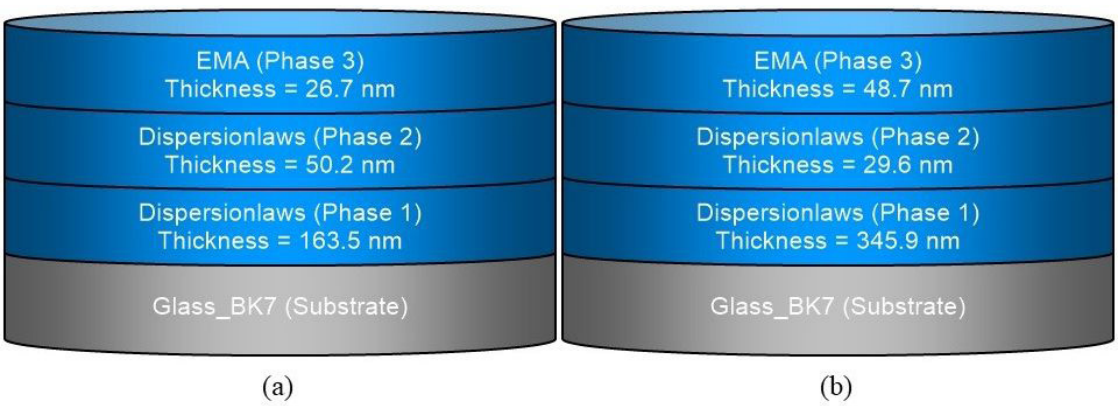

Figure 7. Illustration of the organization of the simulated layers by adjusting the ellipsometric measures of samples A4 (a) and A8 (b).

The thermal lens curves were fitted using the thermal lens model described by Almeida et al[49]. The pumped beam induces excitation, resulting in a phase shift in the probe beam. This phase shift reflects the changes in the optical path length across the entire sample in relation to the trajectory of the probe beam. Variations in the phase shifts were noticed as the nitrogen content was altered in the samples. The thermo-optical parameters are listed in Table 10. The glass substrate did not show a thermal lens signal. Therefore, only the thermo-optical properties of the films were investigated.

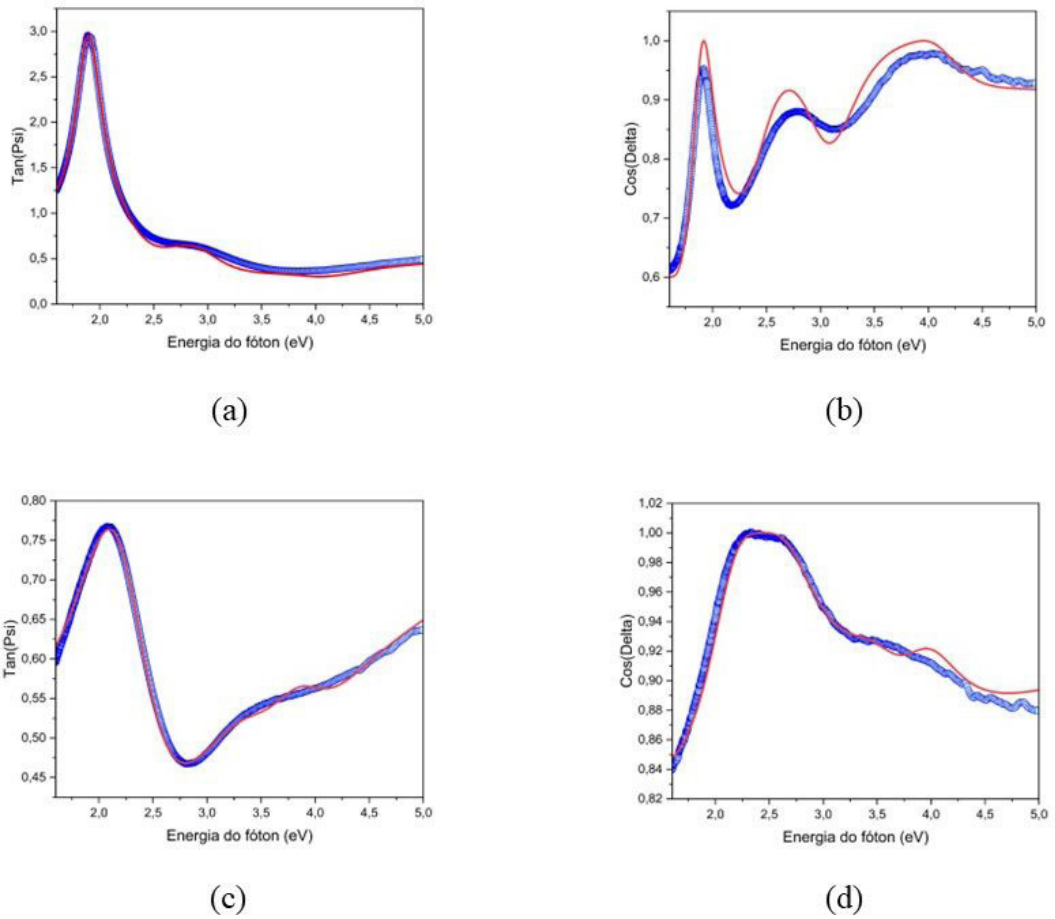

Figure 8. Measurements and ellipsometric adjustments performed on samples A4 (Tan(psi) (a) and Cos(delta) (b)) and A8 (Tan(psi) (c) and Cos(delta) (d)).

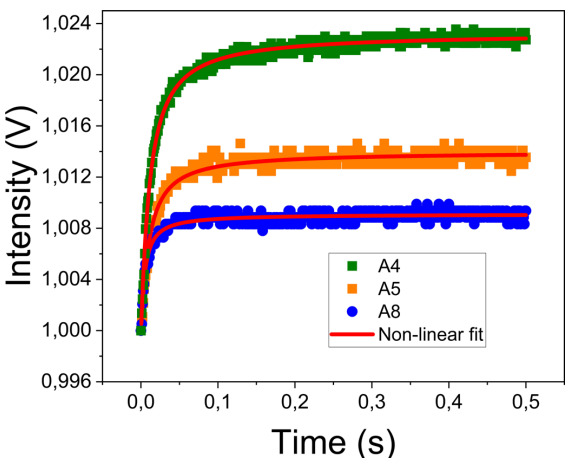

Figure 9. Thermal lens signal for samples A4, A5, and A8.

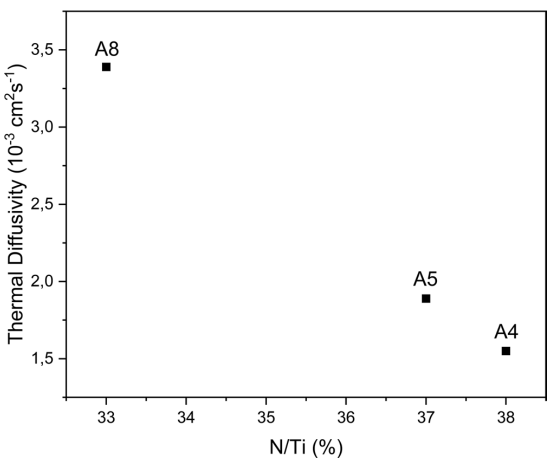

Figure 10. Relationship between the N/Ti ratio and thermal diffusivity.

Table 6. Phase 1 adjusted parameters (thin TiN_x film) resulting from the ellipsometric measurements of samples A4 and A8.

Samples	Fitted Parameters – Phase 1								
	Drude		Lorentz 1			Lorentz 2			Eps_inf
	E_p (eV)	E_Γ (eV)	f	E0 (eV)	Γ (eV)	f	E0 (eV)	Γ (Ev)	
A4	4.42641	0.5	0.51208	2.13897	1.06177	1.14521	5.63981	3.85733	1.7
A8	3.53837	2.67781	1.5302	4.08182	2.11553	2.16528	2.07511	0.90859	1.82682
A17	2.48049	0.35263	2.88834	1.39297	1.08386	1.08386	5.74782	4.71068	2.17034

Table 7. Adjusted parameters of phase 2 (surface layer possibly oxide) resulting from ellipsometric measurements of samples A4 and A8.

Samples	Fitted Parameters - Phase 2							
	Lorentz			Tauc-Lorentz				Eps_inf
	f	E0 (eV)	Γ (Ev)	A (eV)	E0 (eV)	C (eV)	Eg (eV)	
A4	0.30677	2.60806	0.86966	35.65147	4.26671	1.91853	3.90917	2.43327
A8	2.1477	4.24534	3.67622	81.82925	4.02857	1.00033	3.36988	1.40648

Table 8. Parameters derived from the adjustments of the ellipsometric measurements of samples A4 and A8 where phase 3 (EMA) simulates the surface roughness of the sample.

Samples	Fit quality (%)	DERIVED PARAMETERS						
		Phase 2		Phase 1			EMA	
		Thickness (nm)	n @ 632.8	k @ 632.8	Thickness (nm)	n @ 632.8	k @ 632.8	Thickness (nm)
A4	96.2	50.175	1.7958	0.0847	163.548	0.8509	1.4993	26.651
A8	98.7	29.64	2.129	0.2587	345.9	2.425	1.4508	48.69

Table 9. Parameters derived from the adjustments of ellipsometric measures and the total thickness of samples A4 and A8.

Samples	Derived Parameters			Total Thickness (nm)
	Conductivity (S/m)	Resistivity (mΩ.cm)	Resistance (Ω/sq)	
A4	5.2713×10^5	0.1897	11.5995	240.734
A8	6.2894×10^4	1.59	45.9662	424.23

Table 10. Thermo-optical parameters found for samples A4, A5, and A8.

Samples	Phase Difference (rad)	Characteristic Time (s)	Thermal Diffusivity ($cm^2.s^{-1}$)	Thermal Conductivity ($W.K^{-1}.m^{-1}$)
A4	-2.13×10^2	5.80×10^{-4}	1.55×10^{-3}	0.537
A5	-1.26×10^{-2}	4.76×10^{-4}	1.89×10^{-3}	0.655
A8	-8.38×10^{-3}	2.65×10^{-4}	3.39×10^{-3}	1.175

The variation in the proportion of the N:Ar gas mixture of 10, 22, and 50% affected the heat diffusion of the material, with values of 1.55×10^{-3}, 1.89×10^{-3}, and 3.39×10^{-3} $cm^2.s^{-1}$ for the thermal diffusivity for samples A4, A5 and A8, respectively.

Thermal conductivity is proportional to thermal diffusivity. It can be calculated by the following expression, $k=D\rho c$, where ρ is the density and c is the specific heat of the sample. The values of $\rho = 5450$ $kg.m^{-3}$ and $c = 636$ $J.kg^{-1}.K^{-1}$ are already present in the literature[50,51]. The values for the thermal conductivity of the TiN thin films were lower than the same material in bulk, 30 $W.K^{-1}.m^{-1}$ [52]. Figure 10 shows the dependence between thermal diffusivity and the N/Ti ratio, showing that when approaching stoichiometry, there is a decrease in heat diffusion in the material[51,53]. Therefore, the properties and characteristics observed in the films deposited through the different types of analyzes performed indicate that TiN_x thin films deposited through CCPD have the potential to be applied in the development of coatings that act as thermal regulators in smart windows.

4. Conclusions

TiNx substoichiometric thin films were deposited on glass using the CCPD deposition technique. Through Raman measurements, it was possible to estimate the stoichiometry of the films produced. The film deposited with less N_2 flow showed higher stoichiometry than the film deposited with higher N_2 flow. Images obtained through SEM and AFM show the formation of uniform thin films in samples treated with a lower N_2 flow, where the stoichiometry achieved was higher.

This uniformity decreases as the N_2 flow increases and the stoichiometry decreases. The films produced became thicker with increasing partial N_2 flow during deposition. The UV-VIS-NIR spectra indicated that the TiN_x thin films produced with the lowest N_2/Ar ratio had higher stoichiometry (N/Ti ratio of 38%) and reflectivity (30% at 1600 nm), mainly in the near-infrared than those produced with the highest N_2/Ar ratio (N/Ti ratio of 33%), which is promising for the production of heat mirrors or thermally regulated coatings since the deposition method can be improved for such.

The Drude, Lorentz, and Tauc-Lorentz models were applied and refined to better fit the ellipsometric data. The information collected from these adjustments indicated why the transmittance is lower in the UV and visible spectral region and higher in the infrared region since they presented Lorentz bands positioned from 2 to 5.74 eV, indicating light absorption in this spectral range. The higher reflectance in the near-infrared is due to the number of free carriers described by the Drude model, being closely linked to the plasma energy of the material. The more free carriers, the greater the reflectance in that spectral region. Thus, as plasma energy is also closely linked to the stoichiometry of thin films, future studies should address the problem of obtaining stoichiometric and super stoichiometric films.

The analysis using thermal lens spectroscopy showed a strong dependence on the thermal diffusivity of the deposited films and their stoichiometry, where the closer to the stoichiometry the film is, the lower its thermal diffusivity. Thus, the A4 sample showed the highest electrical conductivity and the lowest thermal diffusivity, thus uniting metallic and ceramic properties. This shows that, with a refinement of the method and more profound knowledge of the relationship between the deposition parameters and the general properties of the films produced, it will be possible to develop coatings for thermal regulation to be applied in smart windows. The perspective is that, in the future, coatings produced by this method can add optoelectronic and thermal properties to the treated material, thus expanding the spectrum and quality of its applications.

5. Acknowledgments

This study was partially funded by the Coordination for the Improvement of Higher Education Personnel - Brazil (CAPES) - Financial Code 001.

6. References

1. Dalapati GK, Kushwaha AK, Sharma M, Suresh V, Shannigrahi S, Zhuk S, et al. Transparent heat regulating (THR) materials and coatings for energy saving window applications: impact of materials design, micro-structural, and interface quality on the THR performance. Prog Mater Sci. 2018;95:42-131.
2. Vasiliev M, Nur-E-Alam M, Alameh K. Transparent heat regulation materials and coatings: present status, challenges, and opportunity. In: Dalapati GK, Sharma M, editors. Energy saving coating materials: design, process, implementation and recent developments. Amsterdam: Elsevier; 2020. p. 57-82.
3. Xu K, Du M, Hao L, Mi J, Yu Q, Li S. A review of high-temperature selective absorbing coatings for solar thermal applications. J Materiomics. 2020;6(1):167-82.
4. Zhao Y, Ji H, Lu M, Tao J, Ou Y, Wang Y, et al. Thermochromic smart windows assisted by photothermal nanomaterials. Nanomaterials. 2022;12(21):3865.
5. Dalapati GK, Sharma M. Energy saving coating materials : design, process, implementation and recent developments. Amsterdam: Elsevier; 2020.
6. Khandelwal H, Schenning APHJ, Debije MG. Infrared regulating smart window based on organic materials. Adv Energy Mater. 2017;7(14):1602209.
7. Smith GB, Swift PD, Bendavid A. TiNx films with metallic behavior at high N/Ti ratios for better solar control windows. Appl Phys Lett. 1999;75(5):630-2.
8. Oyama ST, editor. The chemistry of transition metal carbides and nitrides. Dordrecht: Springer Netherlands; 1996.
9. Korpi AG, Ţălu Ş, Bramowicz M, Arman A, Kulesza S, Pszczolkowski B, et al. Minkowski functional characterization and fractal analysis of surfaces of titanium nitride films. Mater Res Express. 2019;6:086463.
10. Choi J, Jeon W, Kang D, Kang D, Jo J. Hydrogen-assisted sputtering growth of TiN on ceramic substrates. Coatings. 2019;9(4):255.
11. Kim HT, Park JY, Park C. Effects of nitrogen flow rate on titanium nitride films deposition by DC facing target sputtering method. Korean J Chem Eng. 2012;29(5):676-9.
12. Schmid PE, Sato Sunaga M, Lévy F. Optical and electronic properties of sputtered TiNx thin films. J Vac Sci Technol A. 1998;16(5):2870-5.
13. Bilokur M, Gentle A, Arnold M, Cortie MB, Smith GB. Optical properties of refractory TiN, AlN and (Ti,Al)N coatings. In: SPIE Micro+Nano Materials, Devices, and Applications; 2015; Sydney, NSW, Australia. Proceedings. Bellingham: SPIE; 2015. (SPIE; 9668).
14. Ye J, Yu J, He H, Zhang Y. Effect of water on wear of phosphate laser glass and BK7 glass. Wear. 2017;376–377:393-402.
15. REALUM [homepage on the Internet]. São Paulo; 2023 [cited 2023 Mar 28]. Available from: https://www.realum.com.br/produto-01c.php
16. Shen J, Soroka AJ, Snook RD. A model for cw laser induced mode-mismatched dual-beam thermal lens spectrometry based on probe beam profile image detection. J Appl Phys. 1995;78(2):700-8.
17. Cheng YH, Tay BK, Lau SP. Influence of deposition temperature on the structure and internal stress of TiN films deposited by filtered cathodic vacuum arc. J Vac Sci Technol A. 2002;20(4):1270.
18. Ding ZH, Yao B, Qiu LX, Lv TQ. Raman scattering investigation of nanocrystalline δ-TiNx synthesized by solid-state reaction. J Alloys Compd. 2006;421(1-2):247-51.
19. Escalona M, Bhuyan H, Ibacache S, Retamal MJ, Saikia P, Borgohain C, et al. Study of titanium nitride film growth by plasma enhanced pulsed laser deposition at different experimental conditions. Surf Coat Tech. 2021;405:126492.
20. Munteanu D, Vaz F. The influence of nitrogen content on the properties of TiN X thin films. J Optoelectron Adv Mater. 2006;8(2):720-5.
21. Schiller S, Beister G, Sieber W. Reactive high rate D.C. sputtering: deposition rate, stoichiometry and features of TiO_x and TiN_x films with respect to the target mode. Thin Solid Films. 1984;111(3):259-68.
22. Vasu K, Kiran MSRN, Krishna MG, Padmanabhan KA. Nitrogen deficiency and metal dopant induced sub-stoichiometry in titanium nitride thin films: a comparative study. Int J Mater Res. 2013;104(9):879-84.
23. Borah SM. Direct Current magnetron glow discharge plasma characteristics study for controlled deposition of titanium nitride thin film. J Mater. 2013;2013:852859.
24. García-González L, Zamora-Peredo L, Flores-Ramírez N, Garnica-Romo MG, Hernández-Torres J. Influence of nitrogen flow rates on the structure, hardness, and electrical resistivity of HfN coatings by DC sputtering. J Mater Eng Perform. 2015;24(4):1558-64.

25. Lee Y-K, Kim J-Y, Lee Y-K, Lee M-S, Kim D-K, Jin D-Y, et al. Surface chemistry of non-stoichiometric TiN_x films grown on (1 0 0)Si substrate by DC reactive magnetron sputtering. J Cryst Growth. 2002;234(2-3):498-504.
26. González-Carmona JM, Triviño JD, Gómez-Ovalle Á, Ortega C, Alvarado-Orozco JM, Sánchez-Sthepa H, et al. Wear mechanisms identification using Kelvin probe force microscopy in TiN, ZrN and TiN/ZrN hard ceramic multilayers coatings. Ceram Int. 2020;46(15):24592-604.
27. Atta S, NarendraKumar U, Kumar KVANPS, Yadav DP, Dash S. Recent developments and applications of TiN-based films synthesized by magnetron sputtering. J Mater Eng Perform. 2023. In press.
28. Jithin MA, Ganapathi KL, Ambresh M, Nukala P, Udayashankar NK, Mohan S. Development of titanium nitride thin film microheaters using laser micromachining. Vacuum. 2022;197:110795.
29. Nimnual P, Sakulkalavek A, Sakdanuphab R. The influence of N_2 partial pressure on color, mechanical, and corrosion properties of TiN thin films deposited by dc reactive magnetron sputtering. Key Eng Mater. 2015;659:550-4.
30. Qi R, Pan L, Feng Y, Wu J, Li W, Wang Z. Evolution of chemical, structural, and mechanical properties of titanium nitride thin films deposited under different nitrogen partial pressure. Results Phys. 2020;19:103416.
31. Das S, Guha S, Ghadai R, Sharma A. Influence of nitrogen gas over microstructural, vibrational and mechanical properties of CVD Titanium nitride (TiN) thin film coating. Ceram Int. 2021;47(12):16809-19.
32. Aissani L, Alhussein A, Ayad A, Nouveau C, Zgheib E, Belgroune A, et al. Relationship between structure, surface topography and tribo-mechanical behavior of Ti-N thin films elaborated at different N_2 flow rates. Thin Solid Films. 2021;724:138598.
33. Pradhaban G, Kuppusami P, Ramachandran D, Viswanathan K, Ramaseshan R. Nanomechanical properties of TiN/ZrN multilayers prepared by pulsed laser deposition. Mater Today Proc. 2016;3(6):1627-32.
34. Morozov IG, Belousova OV, Belyakov OA, Parkin IP, Sathasivam S, Kuznetcov MV. Titanium nitride room-temperature ferromagnetic nanoparticles. J Alloys Compd. 2016;675:266-76.
35. Guo WP, Mishra R, Cheng CW, Wu BH, Chen LJ, Lin MT, et al. Titanium nitride epitaxial films as a plasmonic material platform: alternative to Gold. ACS Photonics. 2019;6(8):1848-54.
36. Cinali MB, Coşkun ÖD. Improved infrared emissivity of diamond-like carbon sandwich structure with titanium nitride metallic interlayer. Sol Energy. 2020;204:644-53.
37. Hu C, Guo K, Li Y, Gu Z, Quan J, Zhang S, et al. Optical coatings of durability based on transition metal nitrides. Thin Solid Films. 2019;688:137339.
38. Chandra R, Chawla AK, Kaur D, Ayyub P. Structural, optical and electronic properties of nanocrystalline TiN films. Nanotechnology. 2005;16(12):3053-6.
39. Mohamed SH, Zhao H, Romanus H, El-Hossary FM, Abo EL-Kassem M, Awad MA, et al. Optical, water splitting and wettability of titanium nitride/titanium oxynitride bilayer films for hydrogen generation and solar cells applications. Mater Sci Semicond Process. 2020;105:104704.
40. Vasu K, Krishna MG, Padmanabhan KA. Substrate-temperature dependent structure and composition variations in RF magnetron sputtered titanium nitride thin films. Appl Surf Sci. 2011;257(7):3069-74.
41. El-Rahman AMA, Mohamed SH, Khan MT, Awad MA. Plasmonic performance, electrical and optical properties of titanium nitride nanostructured thin films for optoelectronic applications. J Mater Sci Mater Electron. 2021;32(24):28204-13.
42. Kaur M, Ishii S, Shinde SL, Nagao T. All-ceramic solar-driven water purifier based on anodized aluminum oxide and plasmonic titanium nitride. Adv Sustainable Syst. 2019;3(2):1800112.
43. Albert P, Narayanan J, Arockiadoss T. Indium-tin oxide regulated band gap of nitrogen-doped titanium oxide thin films for visible light photocatalyst. Appl Phys, A Mater Sci Process. 2021;127(12):900.
44. Kim HJ, Cho YJ, Cho HM, Chegal W, Lee YW, Kim SY. Determination of optical properties of titanium dioxide thin films on different substrates by using spectroscopic ellipsometry. In: SPIE 5538, Optical Constants of Materials for UV to X-Ray Wavelengths; 2004; Denver, CO, USA. Proceedings. Bellingham: SPIE; 2004. p. 165.
45. Mascaretti L, Barman T, Bricchi BR, Münz F, Li Bassi A, Kment Š, et al. Controlling the plasmonic properties of titanium nitride thin films by radiofrequency substrate biasing in magnetron sputtering. Appl Surf Sci. 2021;554:149543.
46. Roquiny P, Bodart F, Terwagne G. Colour control of titanium nitride coatings produced by reactive magnetron sputtering at temperature less than 100°C. Surf Coat Tech. 1999;116-119:278-83.
47. Kurtz SR, Gordon RG. Chemical vapor deposition of titanium nitride at low temperatures. Thin Solid Films. 1986;140(2):277-90.
48. Van Bui H, Kovalgin AY, Wolters RAM. On the difference between optically and electrically determined resistivity of ultra-thin titanium nitride films. Appl Surf Sci. 2013;269:45-9.
49. Almeida AS, Rivera G, Sousa CA, Santos FEP, Souza DN. Thermal lens spectroscopy dosimetry at high doses using a commercial transparent glass. Radiat Meas. 2019;124:85-90.
50. Albert Irudayaraj A, Srinivasan R, Kuppusami P, Mohandas E, Kalainathan S, Ramachandran K. Photoacoustic measurement of thermal properties of TiN thin films. J Mater Sci. 2008;43(3):1114-20.
51. Lopes C, Rodrigues MS, Ferreira A, Macedo F, Borsan I, Gabor C, et al. The influence of the nanostructure design on the optical, electrical and thermal properties of TiNx thin films prepared by reactive magnetron sputtering. Mater Chem Phys. 2023;306:127981.
52. Rohde M. Photoacoustic characterization of thermal transport properties in thin films and microstructures. Thin Solid Films. 1994;238(2):199-206.
53. Lu G, Yu L, Ju H, Zuo B, Xu J. Influence of nitrogen content on the thermal diffusivity of TiN films prepared by magnetron sputtering. Surf Eng. 2020;36(2):192-8.